Title

Hybrid lipid/block copolymer vesicles display broad phase coexistence region

Journal

Biochimica et Biophysica Acta (BBA) - Biomembranes, 1863(4)

ISSN

0005-2736

Authors

Hamada, Naomi
Gakhar, Sukriti
Longo, Marjorie L

Publication Date

2021-04-01

DOI

10.1016/j.bbamem.2021.183552

Peer reviewed

BBA - Biomembranes 1863 (2021) 183552

Contents lists available at ScienceDirect

BBA - Biomembranes

journal homepage: www.elsevier.com/locate/bbamem

Hybrid lipid/block copolymer vesicles display broad phase coexistence region

Naomi Hamada, Sukriti Gakhar, Marjorie L. Longo *

Department of Chemical Engineering, University of California Davis, Davis, CA 95616, United States

ARTICLE INFO

Keywords:
Hybrid vesicles
Membrane phase behavior
Copolymer
Membrane fluidity
Fluorescence spectroscopy

ABSTRACT

The fluidity and polar environment of ~100 nm hybrid vesicles combining dipalmitoylphosphatidylcholine (DPPC) and poly(1,2-butadiene)-*block*-polyethylene oxide (PBd-PEO, average molecular weight 950 g/mol) were studied upon vesicle heating using the fluorescence spectroscopy techniques of DPH anisotropy and laurdan generalized polarization (GP). These techniques indicated PBd-PEO membranes are less ordered than solid DPPC, but slightly more ordered than fluid DPPC or dioleoylphosphatidylcholine (DOPC) membranes. We find the DPH anisotropy values are less than expected from additivity of the components' anisotropies in the fluid phase mixture of DPPC and PBd-PEO, inferring that DPPC strongly fluidizes the PBd-PEO. We use transitions in DPH anisotropy and laurdan GP to create a temperature/composition phase diagram for DPPC/PBd-PEO which we find displays a significantly broader solid/fluid phase coexistence region than DPPC/DOPC, showing that DPPC partitions less readily into fluid PBd-PEO than into fluid DOPC. The existence of a broad solid/fluid phase coexistence region in DPPC/PBd-PEO vesicles is verified by Förster resonance energy transfer results and the visualization of phase separation in giant unilamellar vesicles containing up to 95% PBd-PEO and a single phase in 100% PBd-PEO vesicles at room temperature. These results add to the limited knowledge of phase behavior and phase diagrams of hybrid vesicles, and should be useful in understanding and tailoring membrane surface architecture toward biomedical applications such as drug delivery or membrane protein reconstitution.

1. Introduction

Hybrid vesicles, formed using amphiphilic block copolymers and lipids, combine the advantageous properties of both components and have gained the interest of the scientific community in recent years. While phospholipids are inherently biocompatible, block copolymers offer increased mechanical stability [1,2] and chemical diversity due to their tunable nature. These unique characteristics of hybrid vesicles make them desirable for potential applications in drug delivery and membrane protein reconstitution. Utilization of such hybrid vesicles for these applications requires an understanding of the membrane surface structure (*i.e.* the presence or absence of lipid- and polymer-rich phases), which may impact their efficacy toward the intended function. For example, it has been shown that phase-separated liposomes had an increased efficiency in escaping the endosome for intracellular delivery of cargo [3,4]. Similarly, the activity of certain membrane proteins reconstituted in lipid membranes has been shown to be dependent on bilayer surface heterogeneity [5–8]. Therefore, it is essential to understand and tune the surface morphology of biomembranes for potential biomedical applications.

It is well established that lipid mixtures can demonstrate temperature and composition dependent phase separation driven by the hydrophobic thickness mismatch between different phases. Accordingly, an extensive body of work exists using methods including fluorescence microscopy [9], ^{2}H NMR [10], differential scanning calorimetry (DSC) [11], and fluorescence spectroscopy [12,13] to map the phase diagrams of lipid mixtures. In some recent studies, similar investigations have demonstrated the existence of separate lipid- and polymer- rich phases in hybrid vesicles [2,14–18]. However, the discussion on these phases has been limited to certain compositions and temperatures except for the work of Dao et al. [15] and Chen and Santore [2], which respectively present an apparent phase diagram for a 1-palmitoyl-2-oleoyl-glycero-3-phosphocholine (POPC)/polyethylene oxide-polydimethylsiloxane-polyethylene oxide (PEO-PDMS-PEO) copolymer mixture and a partial range of solid to fluid phase transition temperatures for a mixture of dipalmitoylphosphatidylcholine (DPPC) and a PDMS-PEO copolymer. Formation of hybrid giant unilamellar vesicles (GUVs) formed with polybutadiene-polyethylene oxide (PBd-PEO) block copolymers has

* Corresponding author.
E-mail address: mllongo@ucdavis.edu (M.L. Longo).

https://doi.org/10.1016/j.bbamem.2021.183552
Received 14 September 2020; Received in revised form 29 December 2020; Accepted 4 January 2021
Available online 11 January 2021

demonstrated that certain combinations of the lipids DPPC or POPC with PBd-PEO can display either separate lipid- and polymer-rich domains, or a homogeneous membrane [14,16,19]. PBd-PEO hybrid membranes have also been shown to extend the functional lifetime of an incorporated membrane protein [20]. When used to form hybrid nano-sized vesicles, PDMS-based copolymers have been reported to form stable nanodomains at certain temperatures [21], but such behavior has not yet been fully explored for membranes containing polybutadiene-based copolymers. Thus, there exists an ongoing need to systematically investigate the phase behavior of lipid/polymer mixtures.

Development of a temperature/composition phase diagram mapping the behavior of hybrid vesicles formed using DPPC and poly(butadiene)-*block*-poly(ethylene oxide) (PBd-PEO) is therefore presented here. DPPC is a fully saturated lipid with a main solid-to-fluid phase transition temperature (T_{mid}) of ~41 °C [11]. The PBd-PEO block copolymer used here had an average molecular weight of 950 g/mol (Bd(600)-EO(350)). This polymer is expected to demonstrate relatively fluid behavior across the range of temperatures explored due to the low glass transition temperature of its hydrophobic block [22]. Fluorescence spectroscopy and microscopy are combined to map the phase behavior of hybrid vesicles composed of DPPC and PBd-PEO. To construct an apparent temperature/composition phase diagram for DPPC/PBd-PEO vesicles, delimiting temperatures of large unilamellar vesicles are determined using the fluorescent probes diphenylhexatriene (DPH) and laurdan. Phase behavior is further evaluated by examining the efficiency of Förster resonance energy transfer (FRET).

Observing the temperature- and composition-dependent properties of DPH fluorescence anisotropy and laurdan generalized polarization (GP) values has been previously established as a method to map phase diagrams of lipid mixtures [12,23,24], but to the best of our knowledge has not been applied for this purpose to lipid/copolymer mixtures. Additionally, fluorescence microscopy is used to visualize domain formation in micron scale GUVs. The results presented here suggest the phase diagram for DPPC/PBd(600)-PEO(350) indeed consists of coexisting solid and fluid phases below the main phase transition temperature of the DPPC, and fluidizes above this temperature. These results for DPPC/PBd-PEO vesicles are also compared to DPPC/dioleoylphosphatidylcholine (DOPC) vesicles, which display a broad solid/fluid coexistence region. DOPC in the fluid phase is poorly miscible with solid DPPC. PBd-PEO and DPPC would be expected to demonstrate similarly poor miscibility due to the disordered nature of PBd-PEO at room temperature. We will show that phase separation is observed across a greater range of compositions and temperatures for DPPC/PBd-PEO than DPPC/DOPC, and greater deviations from ideal mixing behavior are also observed within hybrid lipid/copolymer membranes.

2. Materials and methods

2.1. Materials

Dipalmitoylphosphatidylcholine (DPPC), dioleoylphosphatidylcholine (DOPC), 1,2-dilinoleoylphosphatidylcholine (18:2 PC) and 1,2-dilinolenoylphosphatidylcholine (18:3 PC), 1,2-dipalmitoyl-sn-glycero-3-phosphoethanolamine-N-(7-nitro-2-1,3-benzoxadiazol-4-yl) (NBD-DPPE) and 1,2-dioleoyl-sn-glycero-3-phosphoethanolamine-N-(lissamine rhodamine B sulfonyl) (Rh-DOPE) in chloroform were purchased from Avanti Polar Lipids Inc. Poly(1,2-butadiene)-*block*-poly(ethylene oxide) (PBd-PEO) diblock copolymer with an average molecular weight of 950 g/mol (P41807C-BdEO, Bd(600)-*b*-EO(350), PDI = 1.06) was purchased from Polymer Source Inc. 1,6-diphenyl-1,3,5-hexatriene (DPH) was purchased from Acros Organics. 6-dodecanoyl-2-dimethylaminonaphthalene (laurdan) was purchased from AdipoGen Life Sciences. Texas Red DHPE was purchased from Biotium. All water used for experiments was purified with a Barnstead Nanopure System (Barnstead Thermolyne, Dubuque, IA) and had a resistivity ≥17.8 MΩ·cm.

2.2. Preparation of hybrid large unilamellar vesicles (LUVs)

DPPC and PBd-PEO stock solution aliquots at 25 mg/mL in chloroform were stored at −20 °C. To achieve appropriate molar ratios of lipid and polymer mixtures (varying from 100 mol% DPPC to 100 mol% PBd-PEO), calculated volumes of stock solutions were combined in clean glass vials. Chloroform was evaporated under a gentle stream of N_2 to form a uniform dried lipid/polymer thin film. The vials were then kept under vacuum for 4–24 h to remove any residual solvent. The lipid/polymer film was rehydrated to a total lipid+polymer concentration of 2 mg/mL using 20 mM Tris-HCl, 100 mM NaCl (pH 7.4) buffer. The hydrated lipid/polymer mixture was heated to 50–55 °C and then extruded through a 0.1 μm polycarbonate membrane using a mini extruder (Avanti). The temperature of the syringe-extruder assembly was maintained above the lipid phase transition temperature during this step. After extrusion, a dilute solution of hybrid vesicles (100×) was used to analyze size distribution using dynamic light scattering.

2.3. Fluorescence anisotropy and generalized polarization measurements

Phase behavior of the hybrid vesicles with temperature was studied using fluorescence anisotropy (r) of the fluorophore DPH. Hybrid vesicles at a concentration of 0.14 mg/mL were incubated with 5 μL of 200 μM DPH stock solution in ethanol for 45 min in the dark. This is a lipid:probe ratio of roughly 30:1. The anisotropy curve observed with a lipid:probe ratio of 500:1 in hybrid vesicles containing 60% PBd-PEO was consistent with that observed at a lipid:probe ratio of 30:1 (Fig. S6). Fluorescence anisotropy was measured using a JASCO spectrofluorometer from 16 °C to 70 °C at an interval of 2 °C. To obtain DPH anisotropy values, samples were measured at least 5 times at each temperature before ramping to the next temperature; reported DPH anisotropy values are the averages of these measurements. Each vesicle sample was heated only once and used to generate a single anisotropy or GP plot. The sample cuvette was incubated at each temperature for 3 min before taking the measurement. The excitation wavelength was 360 nm and the anisotropy value was measured at 440 nm. DPH anisotropy values are calculated using a ratio of the difference in the parallel and perpendicular light intensity of the emission to the total intensity of the excitation light as shown in Eq. (1),

$$r = \frac{I_{\parallel} - I_{\perp}}{I_{\parallel} + 2I_{\perp}} \tag{1}$$

In order to track the fluidization of the membrane with temperature, least squares regression was used to fit observed anisotropy values to a sigmoidal function (Eq. (2)). r_{max}, r_{min}, n, and T_{mid} are the maximum anisotropy value, minimum anisotropy value, a fitting parameter, and the inflection point of the sigmoidal function respectively. r_{max} and r_{min} establish the upper and lower limits of the anisotropy curve. A and B introduce a quadratic baseline to the function, which may better capture any asymmetry in the anisotropy curve with respect to temperature in the vicinity of T_{mid} for the mixture [25,26].

$$r(T) = \frac{r_{max} - r_{min}}{1 + e^{(T - T_{mid})n}} + r_{min} + AT + BT^2 \tag{2}$$

This approach was also used to evaluate the fluidity indicated by DPH anisotropy for DPPC/DOPC, DPPC/18:2 PC, and DPPC/18:3 PC LUVs (prepared as in Section 2.2), providing a comparison to lipid systems for the phase behavior of hybrid DPPC/PBd-PEO LUVs. The T_{mid} values observed were relatively independent of vesicle type and preparation (Fig. S4 and Table S1).

In addition to DPH anisotropy measurements, which indicate the fluidity of the membrane, the generalized polarization (GP) of laurdan provides information on the hydration of the membrane. Hybrid vesicles at a molar concentration of 0.1 mM were incubated with 5 μL of 200 μM laurdan stock solution in ethanol for 1 h, yielding a lipid:probe ratio of 500:1. GP of the laurdan probe was measured for temperatures between

4 °C and 70 °C at an interval of 2 °C with an incubation time of 3 min at each temperature. Steady-state emission spectra from vesicle samples were collected at these temperatures between 380 nm and 500 nm upon excitation at 340 nm. Laurdan GP values are calculated using the difference in emission intensities at 440 and 490 nm and indicate the overall solvation of the membrane according to Eq. (3),

$$GP = \frac{I_{440} - I_{490}}{I_{440} + I_{490}} \quad (3)$$

Least squares regression was used to fit observed GP values to a sigmoidal function (a modification of Eq. (2) replacing the terms r_{max} and r_{min} with GP_{max} and GP_{min}, respectively):

$$GP(T) = \frac{GP_{max} - GP_{min}}{1 + e^{(T-T_{mid})n}} + GP_{min} + AT + BT^2 \quad (4)$$

2.4. Temperature dependent Förster resonance energy transfer (FRET)

Fluorescent probes NBD-DPPE and Rh-DOPE were included in the hybrid vesicles at 0.1 mol% and 2 mol% respectively. Both probes combined form a FRET pair with NBD-DPPE as donor and Rh-DOPE as the acceptor. Hybrid vesicles were diluted to a final concentration of 0.1 mM prior to fluorescence measurements. Steady-state fluorescence emission spectra of the donor, NBD-DPPE, were recorded in the presence (F), and absence (F_0) of the acceptor Rh-DOPE at temperatures between 4 °C and 70 °C. Samples were excited at 460 nm and the emission spectra were measured between 500 and 650 nm. NBD emission intensities were evaluated at 534 nm when calculating F and F_0. This experiment was also carried out as described above using DPPC/DOPC LUVs (prepared as in Section 2.2).

The fluorescent probes DPH (donor) and Rh-DOPE (acceptor) were also used as a separate FRET pair in hybrid vesicles at 0.2 mol% and 1 mol%, respectively. A stock solution of 200 μM DPH in ethanol was added to a 0.1 mM LUV suspension to achieve the desired concentration and allowed to incubate in the dark for 45 min prior to fluorescence measurements. The volume of ethanol added was always less than 0.25% of the total diluted vesicle preparation. DPH was excited at 360 nm and its emission intensity recorded at 430 nm.

2.5. Preparation of giant unilamellar vesicles (GUVs)

Giant unilamellar vesicles (GUVs) were prepared by electroformation. The desired amounts of DPPC, PBd-PEO, and Texas Red DHPE stocks in chloroform were combined in a clean glass conical vial and diluted to a final concentration of 0.5 mg/mL in 2:1 chloroform: methanol (by volume). A custom built electroformation chamber consisting of parallel platinum electrodes in a polytetrafluoroethylene housing was used. 25 μL of the stock solution was spread over each electrode using a gastight Hamilton syringe, and a gentle stream of N_2 was used to dry the electrodes. The chamber was placed under vacuum for 2–24 h to remove any residual solvent. Glass coverslips were then fixed in place with vacuum grease over the chamber openings. The sealed chamber was filled with water and placed over a water bath of 50–55 °C. A function generator was connected to the electrodes. Vesicle formation was carried out at 3 V, using a frequency of 10 Hz for 30 min, 3 Hz for 15 min, 1 Hz for 7.5 min, and 0.5 Hz for 7.5 min. The chamber was then allowed to cool to room temperature prior to collection of GUVs. GUVs were stored in a plastic conical tube and imaged within 2 h. A small aliquot of GUVs was added to an imaging chamber formed by a glass slide, silicone spacer, and no. 1.5 coverslip. Fluorescence microscopy images were collected using a Nikon Eclipse 80i equipped with a 60× oil immersion objective.

3. Results and discussion

3.1. Fluorescence anisotropy and generalized polarization measurements

The fluorescent probes 1,6-diphenyl-1,3,5-hexatriene (DPH) and 6-dodecanoyl-2-dimethylaminonaphthalene (laurdan) were used to evaluate the phase behavior of hybrid dipalmitoylphosphatidylcholine (DPPC)/polybutadiene-*block*-polyethylene oxide (PBd-PEO) LUVs. Both DPH and laurdan partition strongly into LUV membranes [27,28] and provide insight regarding local membrane properties. LUVs were formed by extrusion and had average diameters ranging from 80 to 120 nm as measured by dynamic light scattering (Table S3). The compositions reported are mole percentages, unless otherwise specified.

DPH fluorescence anisotropy values depend strongly on the fluidity of the membrane into which DPH is incorporated, with high anisotropy values corresponding to a more solid, ordered membrane and low values to a more fluid, disordered membrane [12]. DPH steady state fluorescence anisotropy (DPH anisotropy) values were obtained across a range of temperatures crossing the main phase transition of DPPC, corresponding to the transition from an ordered solid phase to a disordered fluid phase [29]. These results are shown in Fig. 1A for LUVs for a range of DPPC/PBd-PEO compositions. When measured across this range of temperatures DPH anisotropy behaved as a sigmoidal function, decreasing slowly far below and above the main phase transition of DPPC and rapidly in between. As a general trend, incorporating increasing amounts of PBd-PEO shifted this inflection point to lower temperatures, as expected due to the low glass transition temperature of PBd-PEO [22]. DPH anisotropy curves were also observed to be reversible with temperature (Fig. S5) suggesting the temperature ramp rate used was appropriate.

As shown in Fig. 1A, DPH anisotropy values for pure PBd-PEO LUVs do not have the characteristic sigmoidal curve with increasing temperature. This suggests the absence of a phase transition within the observed temperature range, although DPH anisotropy still demonstrates significant dependence on temperature due to an increase in membrane fluidity as the temperature increases [30]. A similar temperature dependence has been previously observed in fluid palmitoyl-oleoyl-phosphatidylcholine (POPC) vesicles [23] and observed by us in pure dioleoylphosphatidylcholine (DOPC) LUVs (Fig. S1) above their main phase transition temperatures.

The dependence of DPH anisotropy on temperature and composition in DPPC/PBd-PEO LUVs also follows similar trends to those observed in DPPC/DOPC LUVs (Fig. S1), measured in order to have a comparison to a well-studied binary lipid system [10,12]. DPH anisotropy values at temperatures below the inflection point vary more with composition in DPPC/DOPC vesicles than in DPPC/PBd-PEO vesicles (from 0.28–0.10 and 0.28–0.22, respectively, at 16 °C as the mole fraction of DPPC, x_{DPPC}, varies from 1 ➔ 0). This suggests DOPC forms a much more fluid membrane than PBd-PEO, despite the disordered state of PBd-PEO. Previous work has suggested pure block copolymer membranes have a higher effective viscosity than pure lipid membranes, as determined by comparing experimentally obtained lateral diffusion coefficients of both species to theoretical predictions [31]. This could be attributed to increased drag at the block copolymer bilayer midplane due to entanglements between the hydrophobic tails of copolymers in opposing monolayers [32]. Indeed, DPH anisotropy values at temperatures above the inflection point vary less with composition in DPPC/DOPC vesicles than in DPPC/PBd-PEO vesicles (from 0.02–0.03 and 0.02–0.05 respectively, at 70 °C as x_{DPPC} goes from 1 ➔ 0). This suggests both fluid DPPC and fluid DOPC form a more fluid membrane than PBd-PEO.

To assess the onset (T_{onset}), inflection point (T_{mid}), and completion temperatures ($T_{completion}$) for the sigmoidal portions of the curves, the observed anisotropy values at each composition were regressed against Eq. (2) (Fig. 1A), directly giving T_{mid}. The derivative of Eq. (2) was evaluated with respect to temperature (Fig. 1B). Because of the sigmoidal shape of the DPH anisotropy curves, this yielded peak-shaped

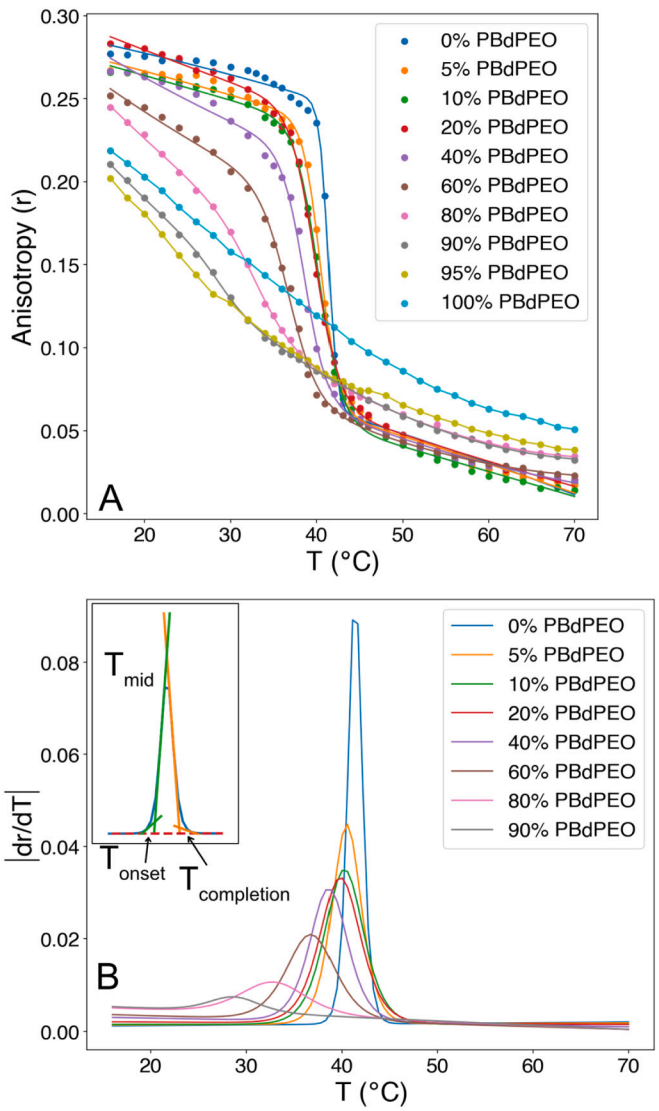

Fig. 1. A. Temperature dependence of DPH anisotropy (r) values in hybrid DPPC/PBd-PEO LUVs. Plotted points correspond to measured data; lines show regressed fits to Eq. (2), except for 95% and 100% PBd-PEO, as Eq. (2) could not be regressed for these compositions due to the lack of clear inflection point. Plotted lines for 95% and 100% PBd-PEO are not the result of any fit. B. The absolute values of the first derivative with respect to temperature of the regressed DPH anisotropy curves. The onset and completion points of the sigmoidal curves were evaluated as shown in the inset: the mean of the intersection with the baseline of lines tangent to the points of steepest slope and of greatest curvature was taken as T_{onset} (green) or $T_{completion}$ (orange). The value of the midpoint temperature, T_{mid}, was obtained by regression of Eq. (2). Inset sample composition is 0% PBd-PEO (100% DPPC).

functions with baseline values corresponding to the small slopes of the DPH anisotropy curves. The points at which the slope begins to deviate sharply from and returns to its baseline values (*i.e.* the start and the end of the peak) correspond T_{onset} and $T_{completion}$. To determine these points, tangent lines were constructed along the peaks shown in Fig. 1B [33]. Representative tangent constructions are shown in Fig. S9. The onset and completion temperatures were taken to be the averages of the intersection of two left-side tangents and two right-side tangents with the baseline of each peak respectively, analogous to the procedure followed to find transition onset and completion temperatures using differential scanning calorimetry (DSC). For pure DPPC LUVs, this yielded a phase transition width of ~5.5 °C and regression against Eq. (2) yielded a T_{mid} of 41.4 ± 0.2 °C (measured by the inflection point in the sigmoidal fit), consistent with values obtained by DSC [11,30,34]. Statistical analysis is discussed in the Supplementary material.

Experimental DPH anisotropy values were compared to the theoretical values using a weighted average, which we will refer to as ideal anisotropy, for different LUV compositions. Ideal anisotropy values were calculated as a weighted sum of the anisotropy values for pure DPPC and pure PBd-PEO LUVs (further discussed in the Supplementary material). Deviations from ideal anisotropy ($\Delta r/r$) (Fig. 2) were then calculated by dividing the difference between observed and ideal anisotropy values by the ideal anisotropy value [35]. Such deviations from ideal anisotropy could be the result of multiple factors. If both DPPC and PBd-PEO coexist within a single phase, deviations from ideal fluidity would suggest the lipid and polymer interact extensively enough to have a fluidizing or an ordering effect on each other. However, if separate DPPC-rich and PBd-PEO-rich phases coexist, interactions with partitioned PBd-PEO or DPPC, respectively, in these phases or contributions of the edges of phase-separated domains could also result in deviations from ideal fluidity.

At temperatures below $T_{completion}$ for LUVs containing ~20–80% PBd-PEO, DPH anisotropy values generally demonstrate small positive deviations from ideal anisotropy, indicating a less fluid membrane than expected. Assuming DPPC-rich solid and PBd-PEO-rich liquid phases coexist below $T_{completion}$, these smaller deviations from ideal anisotropy are not the result of extensive interaction of DPPC and PBd-PEO within one single phase. DPPC might be inducing greater ordering of PBd-PEO by partitioning into the PBd-PEO rich phase and/or by interacting with PBd-PEO partitioning into the DPPC-rich phase. It is also possible that deviations from ideal behavior could be a result of increased ordering at the domain edges.

Above $T_{completion}$, primarily larger, negative deviations from ideal anisotropy are observed, indicating fluid DPPC may have a disordering effect on PBd-PEO. Indeed, above its T_{mid}, pure DPPC displays a lower anisotropy value and greater fluidity than pure PBd-PEO at the same temperatures. The presence of appreciable deviations from ideal anisotropy across this range of temperatures also suggests DPPC and PBd-PEO are able to interact with each other, in turn suggesting the existence of a single fluid phase above $T_{completion}$. While such trends are not as clear above $T_{completion}$ for DPPC/DOPC LUVs (Fig. S7), which consist of a single fluid phase above $T_{completion}$ [10], this may be due to the small difference in the fluidities of pure DPPC and pure DOPC membranes above T_{mid}. A limited dependence of membrane fluidity on composition, and thus weaker deviations from ideal fluidity, would therefore be expected. However, the greater difference in the fluidities of pure DPPC and pure PBd-PEO at these temperatures might facilitate the observation of greater deviations from ideal anisotropy.

For LUVs made with more than 90% PBd-PEO, T_{mid} values could not be resolved due to the absence of clear inflection points in the anisotropy curves; measured anisotropy values for LUVs with these compositions could not be regressed to the expression in Eq. (2). In addition, T_{onset} and $T_{completion}$ could not be clearly resolved for LUVs containing more than 80% PBd-PEO. This motivated the use of laurdan generalized polarization (GP) to provide further data for phase diagram construction, including compositions for which onset, completion, and midpoint temperatures could not be resolved using DPH anisotropy.

Laurdan GP values in DPPC/PBd-PEO LUVs were calculated using Eq. (3). Laurdan displays a red-shifted emission peak in more polar environments [24]. In the case of a lipid membrane undergoing a solid-to-fluid phase transition, an increase in polarity is due to the increase in membrane fluidity permitting increased hydration and thus increased polarity [24]. The dependence of laurdan GP on temperature and vesicle composition indicated similar results to those obtained by evaluating DPH anisotropy values as seen in Fig. 3A. GP behaves as a sigmoidal function of temperature. As greater amounts of PBd-PEO were incorporated, the inflection point of the GP curves shifted to lower temperatures. No phase transition was evident for the pure PBd-PEO membrane. The inflection point of the plot of GP *versus* temperature

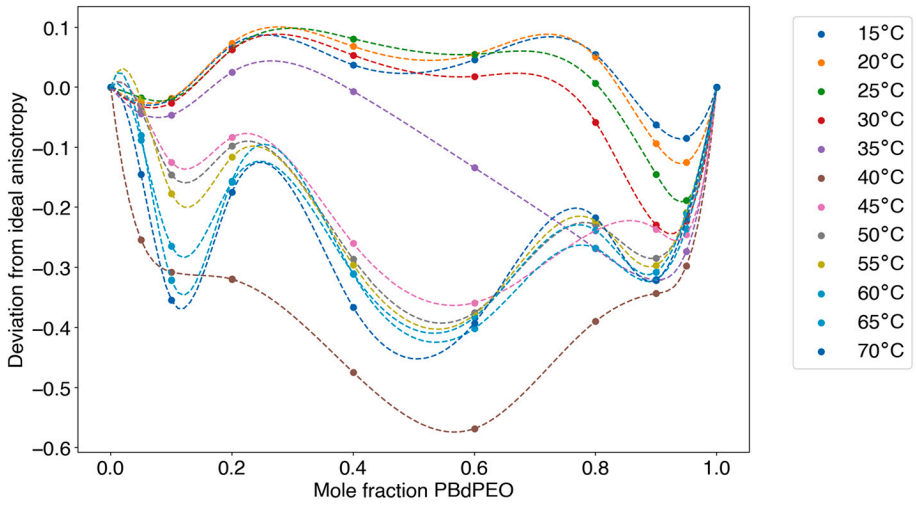

Fig. 2. Deviations from ideal anisotropy ($\Delta r/r$) at select temperatures as a function of DPPC/PBd-PEO LUV composition. Points were calculated as described in the text; dashed lines are cubic splines fit to calculated values.

corresponds to T_{mid}. T_{mid} values were evaluated by regression against a sigmoidal function (Eq. (4)). T_{onset} and $T_{completion}$ values were determined as described for DPH anisotropy values (Fig. S10). For 100% PBd-PEO LUVs, the observed GP values could not be regressed due to the lack of a clear inflection point, so the plotted line in Fig. 3A is included only to guide the eye. T_{mid}, T_{onset}, and $T_{completion}$ could be evaluated for compositions ranging from 0 to 95% PBd-PEO, suggesting greater sensitivity of laurdan than DPH. A much broader transition was observed with laurdan for the pure DPPC LUVs (~9.3 °C), as shown in Fig. 3B, than when DPH was used as the fluorescent probe. However, neither laurdan nor DPH has been found to significantly perturb membrane phase transition behavior [36,37], suggesting this difference does not reflect a true broadening of the phase transition. The $T_{completion}$ values observed were approximately 3 °C higher than those obtained from analysis of DPH fluorescence anisotropy.

3.2. Temperature dependence of FRET efficiency

To obtain further evidence regarding the presence or absence of separate DPPC-rich and PBd-PEO-rich phases in LUVs, the efficiency of FRET between the donor 1,2-dipalmitoyl-sn-glycero-3-phosphoethanolamine-N-(7-nitro-2-1,3-benzoxadiazol-4-yl) (NBD-DPPE) and the acceptor 1,2-dioleoyl-sn-glycero-3-phosphoethanolamine-N-(lissamine rhodamine B sulfonyl) (Rh-DOPE) was evaluated. The Förster radius (R_0) of the NBD/Rh fluorophore pair is approximately 5 nm [38]. Domains smaller than the Förster radius cannot be resolved by FRET and result in a FRET profile indistinguishable from that of a randomly mixed membrane. NBD-DPPE has been found to prefer the ordered phase in DPPC/DOPC/cholesterol mixtures [39], while Rh-DOPE partitions preferentially into the disordered phase due to exclusion of its unsaturated acyl tails from the highly ordered solid phase [40,41]. In the case of fluid/solid phase coexistence, NBD-DPPE and Rh-DOPE would therefore be separated, reducing the efficiency of FRET. Additionally, attempts to conjugate a fluorescent probe to PBd-PEO were unsuccessful, further motivating the use of Rh-DOPE for FRET experiments. To account for the decrease in fluorescence emission intensity often observed with NBD probes at increasing temperature, FRET efficiency was evaluated over a range of temperatures as F/F_0, where F and F_0 are the donor emission intensity in the presence and absence of acceptor, respectively. FRET efficiency is thus $1\text{-}F/F_0$ [42]. Observed trends in F/F_0 are the result of changes in the average proximity of NBD and Rh. For two fluorophores expected to prefer different phases, a higher value of F/F_0 (lower FRET efficiency) would be expected in the case of separate domains. As the ordered phase transitions and the membrane mixes, F/F_0 decreases, resulting in a sigmoidal curve. Each F/F_0 curve was fit with a smoothed cubic spline and the inflection point of the curve was estimated visually to determine T_{mid}. T_{mid} corresponds to the midpoint of the transition from ordered domains large enough to reduce FRET efficiency to domains smaller than the Förster radius of the donor/acceptor pair.

DPPC/PBd-PEO LUVs containing large amounts of PBd-PEO (60–90%) demonstrated a sigmoidal dependence of F/F_0 on temperature (Fig. 4), suggesting the coexistence of separate DPPC-rich and PBd-PEO-rich phases, where ordered DPPC-rich domains decrease in size as the temperature is increased. The inflection points of the F/F_0 curves for these LUVs occur at temperatures as much as 10 °C below the T_{mid} values indicated by DPH anisotropy and laurdan GP curves. As mentioned above, the T_{mid} indicated by FRET represents the midpoint of the temperature range across which ordered domains become too small to be resolved by FRET. Pathak and London have previously reported discrepancies between values of T_{mid} observed with FRET and DPH anisotropy in lipid mixtures. They attributed this to the longer-range nature of FRET interactions (in comparison to DPH anisotropy, which reflects the immediate environment of the probe) [38,43].

FRET efficiency between NBD and Rh was also evaluated in DPPC/DOPC LUVs containing 60% DOPC (Fig. 4) for comparison. While DPH anisotropy indicates a T_{mid} of 29 °C for LUVs of this composition (Fig. S1), FRET indicates a T_{mid} of ~26 °C. For LUVs containing the same amount of PBd-PEO instead of DOPC, FRET indicates a similar T_{mid} of ~27 °C (although DPH anisotropy indicates a higher T_{mid} for LUVs containing 60% PBd-PEO than for those containing 60% DOPC).

To further investigate the extent of domain coexistence in LUVs containing lower concentrations of PBd-PEO, NBD-DPPE was replaced by DPH as the FRET donor to Rh-DOPE (Fig. 5). DPH is expected to partition equally between fluid and solid phases, and the DPH/Rh pair has been reported to have a Förster radius of ~3.6 nm [38]. A sigmoidal F/F_0 curve was observed for LUVs containing 40% PBd-PEO, suggesting coexistence of DPPC-rich and PBd-PEO-rich phases. The inflection point of this curve, corresponding to T_{mid}, was roughly 33.9 °C. This is 4–5 °C below the T_{mid} indicated by DPH anisotropy and laurdan GP—in closer agreement than the 8–10 °C difference between T_{mid} observed in our hybrid membranes with the NBD/Rh FRET pair. Indeed, FRET pairs with smaller Förster radii, which can detect smaller domains, report higher values of T_{mid} [38,43]. In relation to this work, the size of nanodomains in a sphingomyelin/POPC/cholesterol mixture was inferred by comparing the efficiencies of FRET between donor/acceptor pairs with different Förster radii [44].

Above T_{mid}, the low F/F_0 values observed suggest DPPC and PBd-

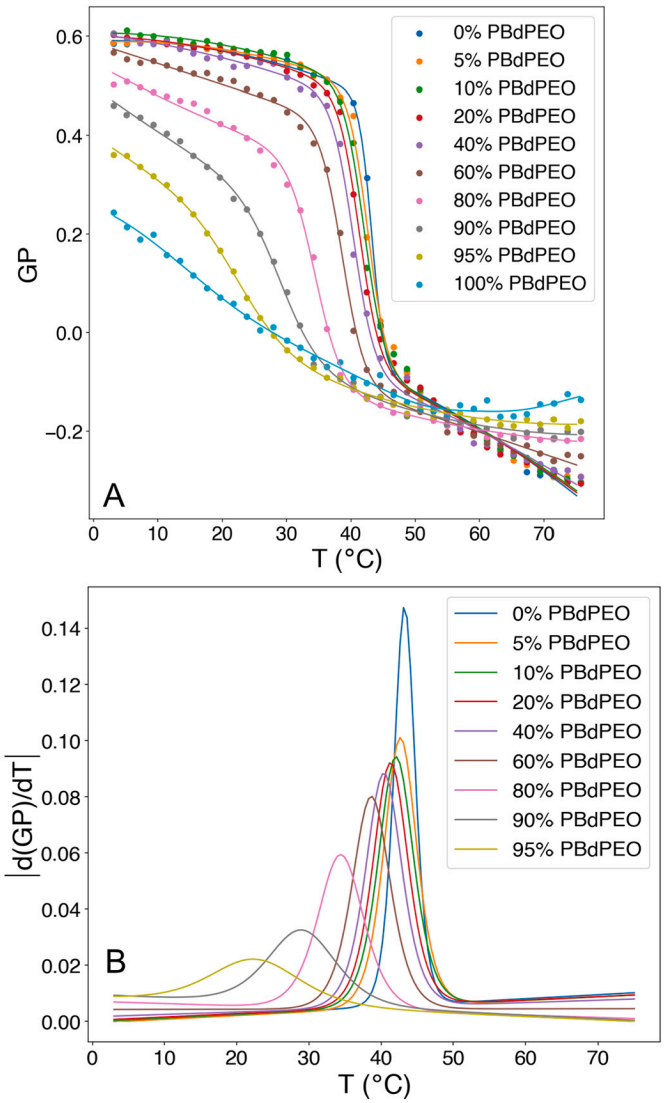

Fig. 3. A. Generalized polarization (GP) of laurdan, corresponding to membrane polarity, as a function of temperature and vesicle composition. GP values were regressed against Eq. (4), except for 100% PBd-PEO, for which no regression could be completed due to the lack of inflection point. Plotted line for 100% PBd-PEO is not the result of any fit. B. Absolute values of the derivatives of the regressed curves in A with respect to temperature.

PEO mix to form a single fluid phase, rather than demonstrating fluid-fluid phase separation (as has been reported for a different lipid/copolymer mixture) [18]. The block copolymer used in this work is expected to have a hydrophobic thickness of ~3 nm [45,46], comparable to that of a fluid lipid membrane. Observation of a single fluid phase above T_{mid} is thus reasonable, as the hydrophobic thickness mismatch between fluid DPPC and PBd-PEO is minimal.

The sigmoidal shape of the F/F_0 curve indicative of a phase transition is largely absent for LUVs containing lower amounts of PBd-PEO (10% and 20%). LUVs containing lower amounts of PBd-PEO have relatively little of the disordered phase, so it is likely that an appreciable amount of Rh-DOPE may also partition into the ordered DPPC-rich phase. This would result in premature quenching of the FRET donor and little change in FRET efficiency once the membrane eventually transitions.

We additionally investigated the effect of Rh-DOPE on the observed T_{mid} in order to ensure the discrepancy between T_{mid} values reported by FRET and DPH anisotropy/laurdan GP is not an artifact from the probe incorporation in the hybrid bilayer. DPH anisotropy and laurdan GP were used to assess T_{mid} in DPPC/PBd-PEO LUVs made with and without

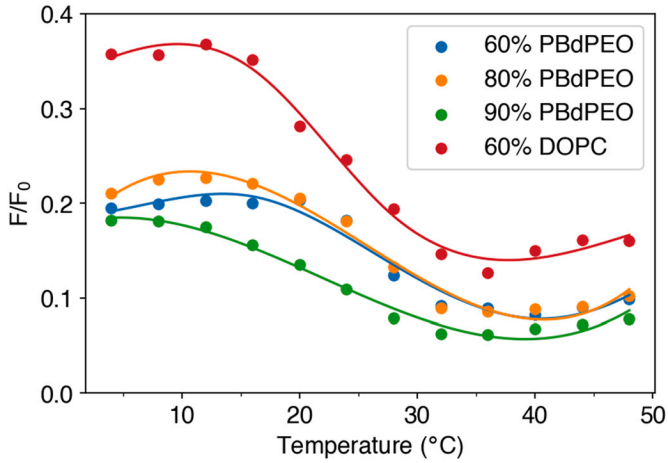

Fig. 4. Efficiency of FRET between NBD-DPPE (0.1 mol%) and Rh-DOPE (2 mol %) in DPPC/PBd-PEO and DPPC/DOPC LUVs. Plotted lines are smoothed cubic splines fit to observed F/F_0 values.

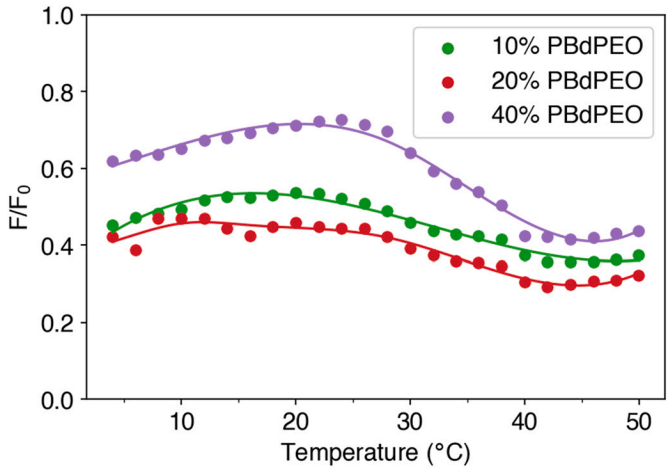

Fig. 5. Efficiency of FRET between DPH (0.2 mol%) and Rh-DOPE (1 mol%) in LUVs made with 10 mol%, 20 mol%, and 40 mol% PBd-PEO between 4 and 50 °C. Plotted lines are smoothed cubic splines fit to each set of F/F_0 values.

Rh-DOPE at the concentrations used for the FRET experiments described above (Fig. S8). DPH anisotropy and laurdan GP reported an increase in T_{mid} of 0.5–1.3 °C upon inclusion of 1% Rh-DOPE, and 0.9–2.2 °C upon inclusion of 2% Rh-DOPE (Table S2), which cannot explain the much lower T_{mid} values reported by FRET in comparison to DPH anisotropy/laurdan GP. Therefore, as discussed earlier, it seems likely that the lower T_{mid} measured using FRET indicates the presence of nanodomains.

3.3. DPPC/PBd-PEO phase diagram and comparisons to GUV behavior

T_{onset}, T_{mid}, and $T_{completion}$ obtained from analysis of DPH anisotropy, laurdan GP, and FRET experiments are summarized in Fig. 6A. The $T_{completion}$ line indicates the endpoint of solid/fluid phase coexistence, *i.e.* the liquidus boundary. At temperatures above $T_{completion}$, solid/fluid phase coexistence gives way to full fluidization of the membrane. The fact that the liquidus line is relatively horizontal between 0% and 60% PBd-PEO suggests the possibility of a coexisting DPPC-rich fluid phase with a PBd-PEO rich fluid phase above this line. Although we label this region as one phase, *i.e.* F(L + P), based on analysis in the previous sections, this is actually still an open question. The solidus boundary on the left side of the phase diagram has been sketched in to mirror the weak partitioning of DPPC into the PBd-PEO-rich phase seen on the right

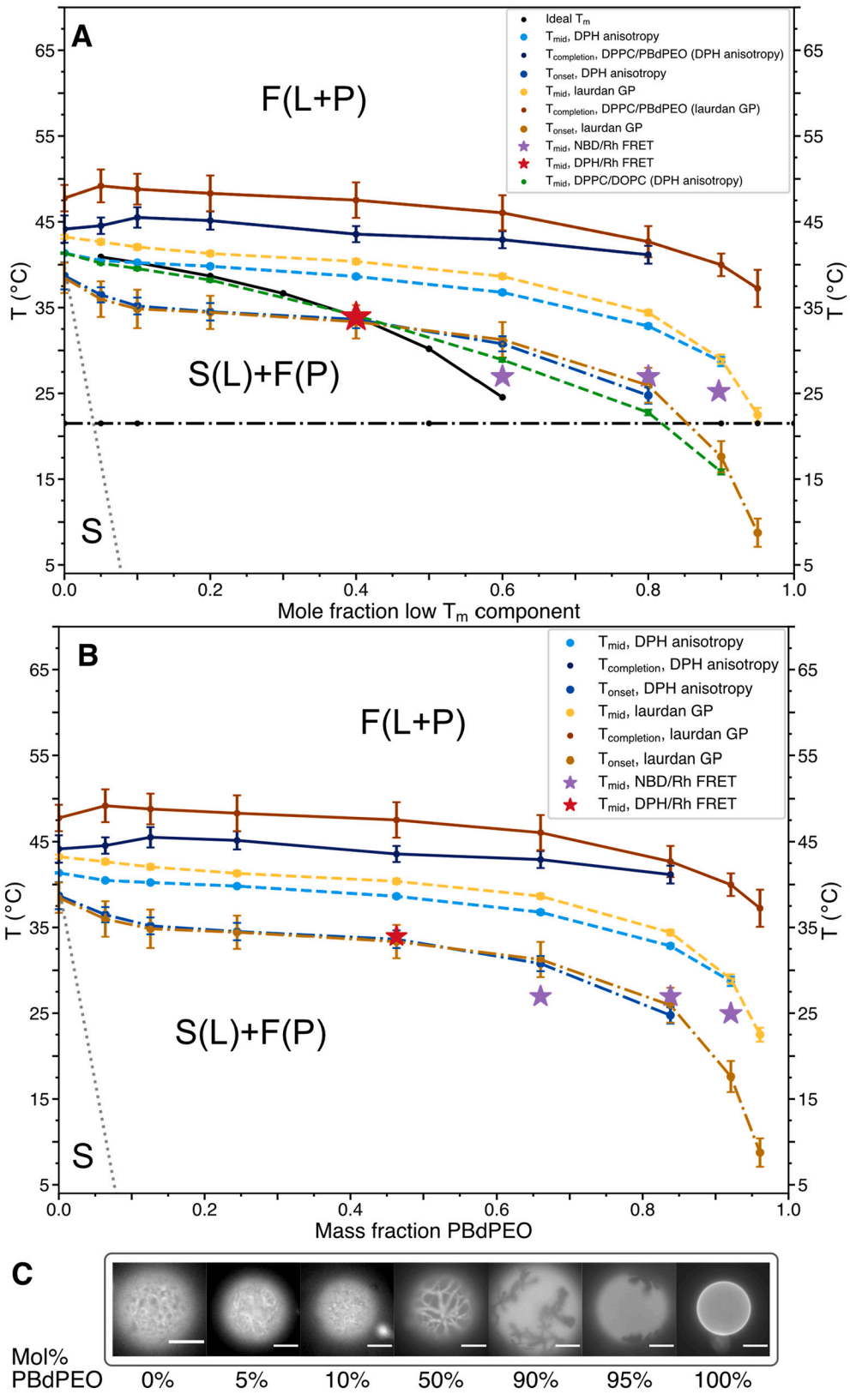

Fig. 6. A. A summary of the onset (T_{onset}), inflection (T_{mid}), and completion ($T_{completion}$) temperatures of the sigmoidal curves indicated by DPH anisotropy, laurdan GP, and FRET between NBD-DPPE/Rh-DOPE or DPH/Rh-DOPE. All data corresponds to DPPC/PBd-PEO vesicles unless otherwise indicated; dashed green line corresponds to DPPC/DOPC vesicles. L and P indicate DPPC lipid-rich and PBd-PEO polymer-rich, respectively; S and F indicate solid and fluid phases. Points obtained by analysis of DPH anisotropy are shown in blue, while points obtained by analysis of laurdan GP are in orange; connecting lines are drawn to guide the eye and not the result of any applied fits. Uncertainty values for 0% PBd-PEO DPH anisotropy data were determined by doubling the propagated standard deviation error for T_{mid} from independent regression of data from 3 samples against Eq. (2). All other error bars represent twice the standard deviation error for the value of T_{mid} returned from regression of measured data from one sample against Eqs. (2) or (4). For $T_{completion}$ and T_{onset}, error bounds were determined as the difference between the intersection of tangent lines to the points of steepest slope and of greatest curvature for the absolute value of the first derivative of the anisotropy or GP values for each composition. For 0% PBd-PEO, this uncertainty was propagated for 3 samples; for all other samples, plotted values represent data from one sample. Dotted gray line is an estimate of the left side of the solidus line. B. Same data as presented in panel A, but with respect to the mass fraction of PBd-PEO instead of the mole fraction. C. Fluorescence microscopy images obtained at room temperature of GUVs labeled with 0.25 mol% Texas Red DHPE, corresponding to the appropriate points on the dot-dashed line in A. Scale bars represent 10 μm.

side of the liquidus line. Both DPH and laurdan results indicate a broad solid/fluid coexistence region (S(L) + F(P)) corresponding to solid DPPC lipid-rich and fluid PBd-PEO polymer-rich phases. The liquidus line has the same shape when plotted with respect to the mass fraction of PBd-PEO (Fig. 6B) which accounts for the possible impact of polymer polydispersity on the actual molar composition.

For comparison, ideal phase transition temperatures for a range of compositions were also sketched by calculating the freezing point depression of DPPC in an ideal mixture of DPPC and PBd-PEO. The molal freezing point depression constant (cryoscopic constant) was calculated

based on an enthalpy of fusion of 8.7 kcal/mol [11] and a van't Hoff factor of 0.5 to account for registry of solid DPPC domains across the bilayer. The large difference in the shape of this line in comparison to the $T_{completion}$ and T_{mid} lines of DPPC/PBd-PEO is a further indication of the non-ideality of the DPPC/PBd-PEO system.

We would expect that the bottom side of the solidus boundary exists at a temperature well below 0 °C as appropriate for PBd-PEO. Therefore, the T_{onset} line is not a solidus line. Indeed, Lentz et al. [12] show a line under the liquidus line, and of the same shape, for DOPC/DPPC membranes measured by DPH anisotropy and interpret it as well within the solid/fluid coexistence region. Based upon their work, it appears that DPH is most sensitive to the fluidity change that takes place in the membrane as it approaches and then crosses the solid/fluid to fluid boundary. Laurdan GP appears to be behaving similarly, as the T_{onset} line closely follows the shape of the $T_{completion}$ line. In contrast, FRET analysis reveals a shift in solid-phase domain size which may be why T_{mid} by FRET (purple stars) may not be following the downward trend of the liquidus line in comparison to T_{mid} for the DPH anisotropy and laurdan GP results, which clearly follow that trend.

Representative fluorescence microscopy images of hybrid GUVs in room-temperature (22 °C ± 2 °C) water are shown in Fig. 6C, corresponding to the labeled points in Fig. 6A. GUVs were formed at 50–55 °C and allowed to cool freely to room temperature (a process typically requiring ~45 min) before being diluted into room temperature water and imaged. GUVs containing as much as 95% PBd-PEO (Fig. 6C) demonstrate clear phase separation indicated by the partitioning of the fluorescently labeled lipid Texas Red DHPE away from solid DPPC-rich (dark) and into fluid PBd-PEO-rich (bright) domains. GUVs containing small amounts of DPPC display irregularly shaped dark domains characteristic of the solid DPPC-rich phase. 50% PBd-PEO GUVs display dark DPPC-rich domains surrounded by bright, interconnected PBd-PEO-rich stripes (Fig. 6C) in approximately equal proportions consistent with the composition on the phase diagram. Previous work studying hybrid lipid/block copolymer GUVs has suggested that at ≥50% DPPC such dark DPPC-rich stripes consist of the gel ($L_{\beta'}$) phase, while patchy domains have been attributed to kinetic trapping of the ripple ($P_{\beta'}$) phase [2]. Pure PBd-PEO GUVs do not demonstrate such phase separation, but instead appear to consist of a single fluid phase (Fig. 6C). This is consistent with the absence of a phase transition indicated by DPH anisotropy and laurdan GP within this temperature range.

The Hildebrand solubility parameter of the polymer hydrophobic block, poly(1,2)-butadiene [47], is reported to be 15.9 $(J/cm^3)^{1/2}$. This solubility parameter is similar for alkanes, typically ranging from ~14–16 $(J/cm^3)^{1/2}$ [48], suggesting the strong tendency for DPPC and PBd-PEO to phase separate does not arise from a fundamental insolubility of the hydrophobic portions of the two components with respect to each other. The PBd-PEO copolymer used in this work has an average molecular weight of 950 g/mol, lighter than those previously studied throughout the literature, which generally range from 1800 to at least 3800 g/mol [16,19,20]. While a smaller hydrophobic mismatch would therefore be expected between DPPC and the lighter PBd-PEO used in this work, as opposed to the heavier copolymers, an extensive two-phase coexistence regime is still observed.

Of note, while DPH anisotropy and laurdan GP suggest DPPC/PBd-PEO bilayers display an extensive solid/fluid phase coexistence region, it is difficult to visually determine whether the inhomogeneity of hybrid GUVs containing smaller amounts of PBd-PEO (*e.g.* 5–10%) is due to phase separation or to the uneven partitioning of Texas Red DHPE (perhaps into the grain boundaries between regions of microcrystalline DPPC-rich solid phase). Indeed, pure DPPC GUVs demonstrate visible inhomogeneity (Fig. 6C), likely for the latter reason.

We also constructed a phase diagram for DPPC/DOPC from our anisotropy data for comparison purposes (Fig. S2) that is in good agreement with that of Lentz et al. [12], when converted to the microviscosity scale used in their work (Fig. S3). For DPPC/PBd-PEO LUVs, $T_{completion}$ decreases only slightly as up to 90% PBd-PEO is added to DPPC, then begins to drop more rapidly as 95% PBd-PEO is approached. In contrast, for DPPC/DOPC LUVs $T_{completion}$ decreases only slightly as up to just 40% DOPC is added to DPPC, as shown in Fig. S2. Beyond this point, $T_{completion}$ then decreases more rapidly as the amount of DPPC decreases for DPPC/DOPC LUVs than for DPPC/PBd-PEO LUVs. Therefore, solid DPPC-rich domains coexist with fluid PBd-PEO-rich domains across a larger range of compositions and temperatures than with fluid DOPC-rich domains as shown in Fig. S2. For example, DPPC/PBd-PEO membranes contain coexisting solid and fluid phases across nearly all compositions at room temperature as shown in Fig. 6, compared to the narrower range of compositions for DPPC/DOPC (Fig. S2). Overall, this comparison shows that while DPPC and PBd-PEO can coexist within hybrid membranes, DPPC partitions less readily into fluid PBd-PEO than into fluid DOPC. Despite this, DPPC appears to have a measurable ordering effect on PBd-PEO based upon the positive deviation from ideal DPH anisotropy discussed in Section 3.1. Moreover, the shape of the T_{mid} line for DPPC/DOPC, shown in Fig. 6A for comparison, follows the ideal freezing point depression line remarkably more closely than for DPPC/PBd-PEO.

We then replaced DOPC with a phosphatidylcholine lipid with two unsaturations in each chain (18:2 PC) and subsequently with a lipid with three unsaturations in each chain (18:3 PC). For mixtures of DPPC and polyunsaturated lipids (DPPC/18:2 PC and DPPC/18:3 PC), the $T_{completion}$ values indicated by DPH anisotropy are very similar to those observed for DPPC/DOPC (Fig. S2). Similar to the addition of DOPC, $T_{completion}$ displays slight decreases as up to 40% of either 18:2 PC or 18:3 PC is added, then decreases more rapidly as more 18:2 PC or 18:3 PC is added. This emphasizes the extensive nature of the DPPC/PBd-PEO phase coexistence region in comparison to the phase behavior observed for mixtures of solely lipids.

4. Conclusions

A combination of fluorescence spectroscopy and microscopy was used to study fluidity and construct a phase diagram for DPPC/PBd-PEO. Fluorescence spectroscopy was also employed to study fluidity and outline a phase diagram for DPPC/DOPC, which was found to be in good agreement with previously published phase diagrams [10,12]. This provided a basis for comparison between the phase behavior of a hybrid lipid/block copolymer membrane and a well-studied lipid system. The liquidus temperatures of DPPC/PBd-PEO display a generally similar dependence on composition to those of DPPC/DOPC, with the liquidus temperature of the mixture decreasing as the amount of the component with the lower phase transition temperature increases. However, DPPC/PBd-PEO displays an expanded solid/fluid phase coexistence region and mixing behavior that is less ideal in comparison to DPPC/DOPC. Solid DPPC partitions less readily into the PBd-PEO-rich fluid phase than into the DOPC-rich fluid phase. While strong negative deviations from ideal anisotropy show that in the fluid region of the phase diagram, fluid DPPC strongly enhances the fluidity of PBd-PEO. Moreover, in the solid-fluid coexistence region, DPPC has a measurable ordering influence on PBd-PEO despite the weak partitioning of DPPC into the PBd-PEO-rich phase. These behaviors reflect that PBd-PEO demonstrates greater fluidity than a solid lipid membrane, but slightly lower fluidity than a fluid lipid membrane. The phase information and diagram developed here may be useful for the design of hybrid biomembranes for drug delivery vehicles or membrane protein reconstitution, given the importance of understanding the membrane phase state for such applications.

Declaration of competing interest

The authors declare that they have no known competing financial interests or personal relationships that could have appeared to influence the work reported in this paper.

Acknowledgements

This material is based upon work supported by the National Science Foundation under Grant No. DMR – 1806366.

Appendix A. Supplementary data

Supplementary data to this article can be found online at https://doi.org/10.1016/j.bbamem.2021.183552.

References

[1] B.M. Discher, Y.-Y. Won, D.S. Ege, J.C.-M. Lee, F.S. Bates, D.E. Discher, D. A. Hammer, Polymersomes: tough vesicles made from diblock copolymers, Science 284 (1999) 1143–1146, https://doi.org/10.1126/science.284.5417.1143.

[2] D. Chen, M.M. Santore, Hybrid copolymer–phospholipid vesicles: phase separation resembling mixed phospholipid lamellae, but with mechanical stability and control, Soft Matter 11 (2015) 2617–2626, https://doi.org/10.1039/C4SM02502D.

[3] Z.I. Imam, L.E. Kenyon, G. Ashby, F. Nagib, M. Mendicino, C. Zhao, A.K. Gadok, J. C. Stachowiak, Phase-separated liposomes enhance the efficiency of macromolecular delivery to the cellular cytoplasm, Cell. Mol. Bioeng. 10 (2017) 387–403, https://doi.org/10.1007/s12195-017-0489-4.

[4] R. Koynova, L. Wang, R.C. MacDonald, Synergy in lipofection by cationic lipid mixtures: superior activity at the gel−liquid crystalline phase transition, J. Phys. Chem. B 111 (2007) 7786–7795, https://doi.org/10.1021/jp071286y.

[5] H. de Lima Santos, M.L. Lopes, B. Maggio, P. Ciancaglini, Na,K-ATPase reconstituted in liposomes: effects of lipid composition on hydrolytic activity and enzyme orientation, Colloids Surf. B: Biointerfaces. 41 (2005) 239–248. doi: https://doi.org/10.1016/j.colsurfb.2004.12.013.

[6] T. Bhatia, F. Cornelius, J. Brewer, L.A. Bagatolli, A.C. Simonsen, J.H. Ipsen, O. G. Mouritsen, Spatial distribution and activity of Na+/K+-ATPase in lipid bilayer membranes with phase boundaries, Biochim. Biophys. Acta Biomembr. 1858 (2016) 1390–1399, https://doi.org/10.1016/j.bbamem.2016.03.015.

[7] B. Cannon, M. Hermansson, S. Györke, P. Somerharju, J.A. Virtanen, K.H. Cheng, Regulation of calcium channel activity by lipid domain formation in planar lipid bilayers, Biophys. J. 85 (2003) 933–942, https://doi.org/10.1016/S0006-3495(03)74532-9.

[8] Ü. Coskun, M. Grzybek, D. Drechsel, K. Simons, Regulation of human EGF receptor by lipids, PNAS. 108 (2011) 9044–9048. doi:https://doi.org/10.1073/pnas.1105666108.

[9] S.L. Veatch, S.L. Keller, Separation of liquid phases in giant vesicles of ternary mixtures of phospholipids and cholesterol, Biophys. J. 85 (2003) 3074–3083, https://doi.org/10.1016/S0006-3495(03)74726-2.

[10] M.L. Schmidt, L. Ziani, M. Boudreau, J.H. Davis, Phase equilibria in DOPC/DPPC: conversion from gel to subgel in two component mixtures, J. Chem. Phys. 131 (2009), 175103, https://doi.org/10.1063/1.3258077.

[11] S. Mabrey, J.M. Sturtevant, Investigation of phase transitions of lipids and lipid mixtures by sensitivity differential scanning calorimetry, PNAS 73 (1976) 3862–3866, https://doi.org/10.1073/pnas.73.11.3862.

[12] B.R. Lentz, Y. Barenholz, T.E. Thompson, Fluorescence depolarization studies of phase transitions and fluidity in phospholipid bilayers. 2. Two-component phosphatidylcholine liposomes, Biochemistry 15 (1976) 4529–4537, https://doi.org/10.1021/bi00665a030.

[13] F.A. Heberle, J.T. Buboltz, D. Stringer, G.W. Feigenson, Fluorescence methods to detect phase boundaries in lipid bilayer mixtures, Biochimica et Biophysica Acta (BBA) - Molecular Cell Research 1746 (2005) 186–192, https://doi.org/10.1016/j.bbamcr.2005.05.008.

[14] J. Nam, T.K. Vanderlick, P.A. Beales, Formation and dissolution of phospholipid domains with varying textures in hybrid lipo-polymersomes, Soft Matter 8 (2012) 7982–7988, https://doi.org/10.1039/c2sm25646k.

[15] T.P.T. Dao, F. Fernandes, E. Ibarboure, K. Ferji, M. Prieto, O. Sandre, J.-F. Le Meins, Modulation of phase separation at the micron scale and nanoscale in giant polymer/lipid hybrid unilamellar vesicles (GHUVs), Soft Matter 13 (2017) 627–637, https://doi.org/10.1039/C6SM01625A.

[16] C. Magnani, C. Montis, G. Mangiapia, A.-F. Mingotaud, C. Mingotaud, C. Roux, P. Joseph, D. Berti, B. Lonetti, Hybrid vesicles from lipids and block copolymers: phase behavior from the micro- to the nano-scale, Colloids Surf. B: Biointerfaces 168 (2018) 18–28, https://doi.org/10.1016/j.colsurfb.2018.01.042.

[17] M. Schulz, D. Glatte, A. Meister, P. Scholtysek, A. Kerth, A. Blume, K. Bacia, W. H. Binder, Hybrid lipid/polymer giant unilamellar vesicles: effects of incorporated biocompatible PIB–PEO block copolymers on vesicle properties, Soft Matter 7 (2011) 8100–8110, https://doi.org/10.1039/C1SM05725A.

[18] T.P.T. Dao, F. Fernandes, M. Er-Rafik, R. Salva, M. Schmutz, A. Brûlet, M. Prieto, O. Sandre, J.-F. Le Meins, Phase separation and nanodomain formation in hybrid polymer/lipid vesicles, ACS Macro Lett. 4 (2015) 182–186, https://doi.org/10.1021/mz500748f.

[19] J. Nam, P.A. Beales, T.K. Vanderlick, Giant phospholipid/block copolymer hybrid vesicles: mixing behavior and domain formation, Langmuir 27 (2011) 1–6, https://doi.org/10.1021/la103428g.

[20] S. Khan, M. Li, S.P. Muench, L.J.C. Jeuken, P.A. Beales, Durable proteo-hybrid vesicles for the extended functional lifetime of membrane proteins in bionanotechnology, Chem. Commun. 52 (2016) 11020–11023, https://doi.org/10.1039/C6CC04207D.

[21] T.P.T. Dao, A. Brûlet, F. Fernandes, M. Er-Rafik, K. Ferji, R. Schweins, J.-P. Chapel, A. Fedorov, M. Schmutz, M. Prieto, O. Sandre, J.-F. Le Meins, Mixing block copolymers with phospholipids at the nanoscale: from hybrid polymer/lipid wormlike micelles to vesicles presenting lipid nanodomains, Langmuir 33 (2017) 1705–1715, https://doi.org/10.1021/acs.langmuir.6b04478.

[22] A.F. Halasa, J.M. Massie, Polybutadiene, in: Kirk-Othmer Encyclopedia of Chemical Technology, John Wiley & Sons, Inc, 2000, https://doi.org/10.1002/0471238961.1615122508011201.a01.

[23] R.F.M. de Almeida, A. Fedorov, M. Prieto, Sphingomyelin/phosphatidylcholine/cholesterol phase diagram: boundaries and composition of lipid rafts, Biophys. J. 85 (2003) 2406–2416, https://doi.org/10.1016/S0006-3495(03)74664-5.

[24] T. Parasassi, G. De Stasio, A. d'Ubaldo, E. Gratton, Phase fluctuation in phospholipid membranes revealed by Laurdan fluorescence, Biophys. J. 57 (1990) 1179–1186, https://doi.org/10.1016/S0006-3495(90)82637-0.

[25] S.C. Nelson, S.K. Neeley, E.D. Melonakos, J.D. Bell, D.D. Busath, Fluorescence anisotropy of diphenylhexatriene and its cationic Trimethylamino derivative in liquid dipalmitoylphosphatidylcholine liposomes: opposing responses to isoflurane, BMC Biophys. 5 (2012) 5, https://doi.org/10.1186/2046-1682-5-5.

[26] W.F. Zeno, S. Hilt, K.K. Aravagiri, S.H. Risbud, J.C. Voss, A.N. Parikh, M.L. Longo, Analysis of lipid phase behavior and protein conformational changes in nanolipoprotein particles upon entrapment in sol–gel-derived silica, Langmuir 30 (2014) 9780–9788, https://doi.org/10.1021/la5025058.

[27] M. Shinitzky, Y. Barenholz, Dynamics of the hydrocarbon layer in liposomes of lecithin and sphingomyelin containing dicetylphosphate, J. Biol. Chem. 249 (1974) 2652–2657.

[28] T. Parasassi, G. De Stasio, G. Ravagnan, R.M. Rusch, E. Gratton, Quantitation of lipid phases in phospholipid vesicles by the generalized polarization of Laurdan fluorescence, Biophys. J. 60 (1991) 179–189, https://doi.org/10.1016/S0006-3495(91)82041-0.

[29] M.R. Vist, J.H. Davis, Phase equilibria of cholesterol/dipalmitoylphosphatidylcholine mixtures: deuterium nuclear magnetic resonance and differential scanning calorimetry, Biochemistry 29 (1990) 451–464, https://doi.org/10.1021/bi00454a021.

[30] B.R. Lentz, Y. Barenholz, T.E. Thompson, Fluorescence depolarization studies of phase transitions and fluidity in phospholipid bilayers. 1. Single component phosphatidylcholine liposomes, Biochemistry 15 (1976) 4521–4528, https://doi.org/10.1021/bi00665a029.

[31] J.C.-M. Lee, M. Santore, F.S. Bates, D.E. Discher, From membranes to melts, rouse to reptation: diffusion in polymersome versus lipid bilayers, Macromolecules 35 (2002) 323–326, https://doi.org/10.1021/ma0112063.

[32] R. Dimova, U. Seifert, B. Pouligny, S. Förster, H.-G. Döbereiner, Hyperviscous diblock copolymer vesicles, Eur. Phys. J. E. 7 (2002) 241–250, https://doi.org/10.1140/epje/i200101032.

[33] J. Ehrig, E.P. Petrov, P. Schwille, Phase separation and near-critical fluctuations in two-component lipid membranes: Monte Carlo simulations on experimentally relevant scales, New J. Phys. 13 (2011), 045019, https://doi.org/10.1088/1367-2630/13/4/045019.

[34] R.L. Biltonen, D. Lichtenberg, The use of differential scanning calorimetry as a tool to characterize liposome preparations, Chem. Phys. Lipids 64 (1993) 129–142, https://doi.org/10.1016/0009-3084(93)90062-8.

[35] M.M. Lozano, M.L. Longo, Complex formation and other phase transformations mapped in saturated phosphatidylcholine/DSPE-PEG2000 monolayers, Soft Matter 5 (2009) 1822, https://doi.org/10.1039/b820070j.

[36] J. Repáková, J.M. Holopainen, M.R. Morrow, M.C. McDonald, P. Čapková, I. Vattulainen, Influence of DPH on the structure and dynamics of a DPPC bilayer, Biophys. J. 88 (2005) 3398–3410, https://doi.org/10.1529/biophysj.104.055533.

[37] S.S.W. Leung, J. Thewalt, Link between fluorescent probe partitioning and molecular order of liquid ordered-liquid disordered membranes, J. Phys. Chem. B 121 (2017) 1176–1185, https://doi.org/10.1021/acs.jpcb.6b09325.

[38] P. Pathak, E. London, The effect of membrane lipid composition on the formation of lipid ultrananodomains, Biophys. J. 109 (2015) 1630–1638, https://doi.org/10.1016/j.bpj.2015.08.029.

[39] J. Juhasz, J.H. Davis, F.J. Sharom, Fluorescent probe partitioning in giant unilamellar vesicles of 'lipid raft' mixtures, Biochem. J. 430 (2010) 415–423, https://doi.org/10.1042/BJ20100516.

[40] T. Baumgart, G. Hunt, E.R. Farkas, W.W. Webb, G.W. Feigenson, Fluorescence probe partitioning between Lo/Ld phases in lipid membranes, Biochim. Biophys. Acta Biomembr. 1768 (2007) 2182–2194, https://doi.org/10.1016/j.bbamem.2007.05.012.

[41] P. Sengupta, A. Hammond, D. Holowka, B. Baird, Structural determinants for partitioning of lipids and proteins between coexisting fluid phases in giant plasma membrane vesicles, Biochim. Biophys. Acta Biomembr. 1778 (2008) 20–32, https://doi.org/10.1016/j.bbamem.2007.08.028.

[42] B.K.-K. Fung, L. Stryer, Surface density determination in membranes by fluorescence energy transfer, Biochemistry 17 (1978) 5241–5248, https://doi.org/10.1021/bi00617a025.

[43] P. Pathak, E. London, Measurement of lipid nanodomain (raft) formation and size in sphingomyelin/POPC/cholesterol vesicles shows TX-100 and transmembrane helices increase domain size by coalescing preexisting nanodomains but do not induce domain formation, Biophys. J. 101 (2011) 2417–2425, https://doi.org/10.1016/j.bpj.2011.08.059.

[44] R.S. Petruzielo, F.A. Heberle, P. Drazba, J. Katsaras, G.W. Feigenson, Phase behavior and domain size in sphingomyelin-containing lipid bilayers, Biochim.

Biophys. Acta Biomembr. 1828 (2013) 1302–1313, https://doi.org/10.1016/j.bbamem.2013.01.007.
[45] G. Srinivas, D.E. Discher, M.L. Klein, Self-assembly and properties of diblock copolymers by coarse-grain molecular dynamics, Nat. Mater. 3 (2004) 638–644, https://doi.org/10.1038/nmat1185.
[46] D.R. Barden, H. Vashisth, Parameterization and atomistic simulations of biomimetic membranes, Faraday Discuss. 209 (2018) 161–178, https://doi.org/10.1039/C8FD00047F.
[47] A.F.M. Barton, Handbook of Polymer-liquid Interaction Parameters and Solubility Parameters, CRC Press, 1990.
[48] A.F.M. Barton, CRC Handbook of Solubility Parameters and Other Cohesion Parameters, 2nd ed., Routledge, 2017 https://doi.org/10.1201/9781315140575.